Scientific Research Publishing

American Journal of Plant Sciences, 2023, 14, 220-245
https://www.scirp.org/journal/ajps
ISSN Online: 2158-2750
ISSN Print: 2158-2742

CO_2 Demand-Supply Coordination in Photosynthesis Reflecting the Plant-Environment Interaction: Extension and Parameterization of Demand Function and Supply Function

Lei Wang[1,2], Qing-Lai Dang[1*]

[1]Faculty of Natural Resources Management, Lakehead University, Thunder Bay, Canada
[2]College of Biotechnology, Jiangsu University of Science and Technology, Zhenjiang, China
Email: *qdang@lakeheadu.ca

How to cite this paper: Wang, L. and Dang, Q.-L. (2023) CO_2 Demand-Supply Coordination in Photosynthesis Reflecting the Plant-Environment Interaction: Extension and Parameterization of Demand Function and Supply Function. *American Journal of Plant Sciences*, **14**, 220-245.
https://doi.org/10.4236/ajps.2023.142017

Received: November 17, 2022
Accepted: February 25, 2023
Published: February 28, 2023

Abstract

Photosynthesis consists of a biochemical process named demand and a CO_2 diffusion process named supply function. The intersection (C_i, A_n) at equal to the demand function and the supply function reflects a steady state of the plant subjected to the environment. The intersections of these demand-supply functions under different photosynthetically active radiation (PAR) can be fitted to a regression line (names DSF) in which slope ($\Delta A_n/\Delta C_i$) can be defined as *dsf*. We found that DSF information was embedded in both Laisk method (CO_2 response curve (A/C_i) measured at three sub-saturated PARs, and their intersections were used to estimate daytime respiration (R_d), and CO_2 compensation point (C_i^*) and light response curve measurements, which could be used to estimate *dsf* values. This study investigated the relationship between *dsf* and the parameters related to the biochemical process and the CO_2 diffusion process of photosynthesis. The results showed that *dsf* was negatively correlated with g_s, apparent carboxylation efficiency, and apparent quantum yield. This suggests that DSF may coordinate the influence of environmental conditions (light, CO_2 and water) on photosynthesis in the biochemical and CO_2 diffusion process. Moreover, *dsf* was independent of gas exchange measurement conditions and showed species specificity. In conclusion, we speculated that *dsf* seems to be a comprehensive parameter that might be related to the intrinsic adaptation mechanism of plants to environmental conditions. We proposed an auxiliary line perpendicular to the DSF and used it to improve the stability of C_i^* and R_d estimated from the Laisk dataset.

Keywords

Photosynthesis, Gas Exchange Measurement, Demand Function, Supply Function, Laisk Method, Light Response Curve

1. Introduction

In the research of plant response to the environment, it is often necessary to investigate the responses of photosynthetic traits, such as phytoremediation of pollutants, saline, ozone stress, climate change [1] [2] [3] [4]. However, the complex processes of photosynthesis are affected by many other internal and external factors/processes such as water relations, lights, energy balance, low and high lights, and nitrogen metabolism [5]. Moreover, CO_2 fixation, mitochondrial respiration and photorespiration involve processes where CO_2 fluxes occur simultaneously [6], making the investigation of photosynthesis under different environmental conditions very challenging and often leading to the over-parameterization of photosynthetic models [7]. Some of the model parameters are difficult to estimate, such as CO_2 compensation point (C_i^*), daytime respiration (R_d), mesophyll conductance (g_m) [8] (**Table 1**). Furthermore, multiple parameters are needed to comprehensively describe the responses of photosynthesis to the environment [9].

Photosynthesis can be roughly divided into two components, the biochemical process, and the CO_2 diffusion process [2] [10] [11]. The biochemical process includes Rubisco carboxylation, the regeneration of CO_2 receptor RuBP, and utilization and transport of photosynthates [12]. The FvCB photosynthesis model is based on Rubisco enzyme kinetics and biochemical metrology [13] and is widely used to scale photosynthesis from chloroplast and leaf level to ecosystem and global levels, such as in the Earth System Models [14]. The parameters involved in the biochemical process include the maximum rate of RuBP carboxylation (V_{cmax}), maximum photosynthetic electron transport rate (J_{max}), apparent carboxylation efficiency (ACE, estimated from A/C_i), and apparent quantum yield (AQY, estimated from light response curve (LRC) (**Table 1**) [15]. The Ball Berry type models have established a linear relationship between net photosynthetic rate (A_n) and stomatal conductance (g_s) to incorporate the CO_2 diffusion process ($g_s = g_0 + g_1 \times A_n \times f(D)/C_a$) [16]. Parameters related to CO_2 diffusion include g_s and mesophyll conductance (g_m) (**Table 1**) [17]. Although these models provide a good explanation of photosynthetic responses to specific environmental factors, the mechanisms and parameters that coordinate biochemical and CO_2 diffusion simultaneously are rarely reported. The actual growth environment conditions are complex and variable, particularly under the scenario of climate change [18].

The biochemical model FvCB of photosynthesis explains the demand function of photosynthesis, while the CO_2 diffusion model Ball-Berry describes the supply

Table 1. Definition of abbreviation.

Acronyms	Definitions	Unit
$\Delta A_n/\Delta C_i$	Ratio of A_n variation to C_i variation with different PAR	-
A/C_i	Net photosynthesis rate vs. CO_2 response curve	-
ACE	Apparent carboxylation efficiency	-
A_n	Net photosynthesis rate	$\mu mol \cdot m^{-2} \cdot s^{-1}$
AQY	Apparent quantum yield	-
bp	Balsam poplar (*Populus balsamifera* L.)	-
C_a	Ambient CO_2 concentration	$\mu mol \cdot mol^{-1}$
CAU	Carbonic anhydrase activity	EU
CEi	Intrinsic carboxylation efficiency	-
C_i	Intercellular CO_2 concentration	$\mu mol \cdot mol^{-1}$
C_i^*	Intercellular CO_2 In Intercellular CO_2 compensation point	$\mu mol \cdot mol^{-1}$
C_i/C_a	Intercellular (C_i) to ambient (C_a) CO^2 concentration ratio	-
CV	Coefficient of variation	-
cw	Black cottonwood (*Populus trichocarpa* Torr. & Gray)	-
DSF	Regression line fitted from the intersections of Demand and Supply Functions under different PAR with a C_a	-
dsf	Slope of DSF ($dsf = \Delta A_n/\Delta C_i$)	-
g_m	Mesophyll conductance	$mol \cdot m^{-2} \cdot s^{-1}$
J_{max}	Maximum photosynthetic electron transport rate	$\mu mol \cdot m^{-2} \cdot s^{-1}$
LRC (or *lrc*)	Light response curve	-
I_v	Vertical line of DSF	-
MP	Conventional average mid-point to estimate R_d and C_i^* from Laisk dataset	-
PAR	Photosynthetically active radiation	$\mu mol \cdot m^{-2} \cdot s^{-1}$
R_d	Daytime respiration	$\mu mol \cdot m^{-2} \cdot s^{-1}$
SI	Slope-intercept method to estimate Rd and C_i^* from Laisk dataset (Walker et al., 2016)	-
V_{cmax}	Maximum rate of RuBP carboxylation	$\mu mol \cdot m^{-2} \cdot s^{-1}$
VL	Novel vertical line (I_v) method to estimate R_d and C_i^* from Laisk dataset	-
wb	White birch (*Betula papyrifera* Marsh.)	-

function of photosynthesis (**Figure 1(a)**) [10]. The demand function is the relationship between net CO_2 assimilation rate and CO_2 concentration inside the leaf (A/C_i response curve) or in the chloroplast (A/C_c response curve); The supply function is the line connecting the ambient on the X-axis (C_a) to the corresponding internal CO_2 concentration on the A/C_i or A/C_c (*i.e.*, C_i or C_c) with the corresponding diffusion conductance to CO_2 as the slope [19]. The actual net photosynthetic rate (A_n) is the rate at the intersection of the two functions [10] [20], as shown in **Figure 1(a)**. We know that RuBP regeneration depends on light-driven electron transport and Rubisco activity. CO_2 diffusion is mainly controlled by g_s, which itself is influenced by the environment (such as soil moisture condition and atmospheric water vapor pressure deficit) [10]. The demand and supply functions together can integrate the physical, biochemical and photochemical limitations to CO_2 diffusion and assimilation at different segments of the photosynthetic pathway, including the CO_2 assimilation capacity in the chloroplast [19] [21]. Therefore, the demand function and supply functions of photosynthesis should reflect the coordination between plants and multiple environmental factors. However, there is still a lack of suitable and easy-to-measure parameters to represent the actual coordination between CO_2 demand and supply in the photosynthetic process.

The supply function and demand function of photosynthesis are not only embedded in the A/C_i curve but also in other photosynthetic measurements such as the Laisk measurement [22]. The Laisk method is used to determine CO_2 compensation points and daytime mitochondrial respiration in the leaf. The method uses photosynthetic CO_2 response curves at low CO_2 concentrations (*i.e.*, the initial part of the A/C_i) measured under three sub-saturation light intensities [23]. According to the FvCB model, the three truncated-A/C_i curves should theoretically intersect each other at a common point where the X and Y values are the intercellular CO_2 compensation point (C_i^*) and the daytime respiration (R_d), respectively [24]. The intersections of the supply function and the demand function with the same C_a be fitted into a regression line (**Figure 1(b)**). The analysis of the coordination between demand function and supply function may help us to better understand the responses of photosynthesis changes in environmental conditions.

Photosynthesis is catalyzed by Rubisco with CO_2 and RuBP as substrates and the photosynthetic rate is the CO_2 fixation rate under a given photosynthetically active radiation (PAR) and C_a. Theoretically, there should be a parameter or parameters that describe the intrinsic photosynthetic traits for a given leaf [25]. However, V_{cmax} and J_{max} do not represent the actual photosynthesis capacity of the leaf [26] [27], The maximum apparent carboxylation efficiency (ACE) is the initial slope of the A/C_i curve at a given PAR, which is related to Rubisco activity [28] [29]. The initial slope of the photosynthetic light response curve (A/L curve) represents the maximum apparent quantum yield (AQY) under the measurement C_a, which is generally considered to be related to photorespiration or

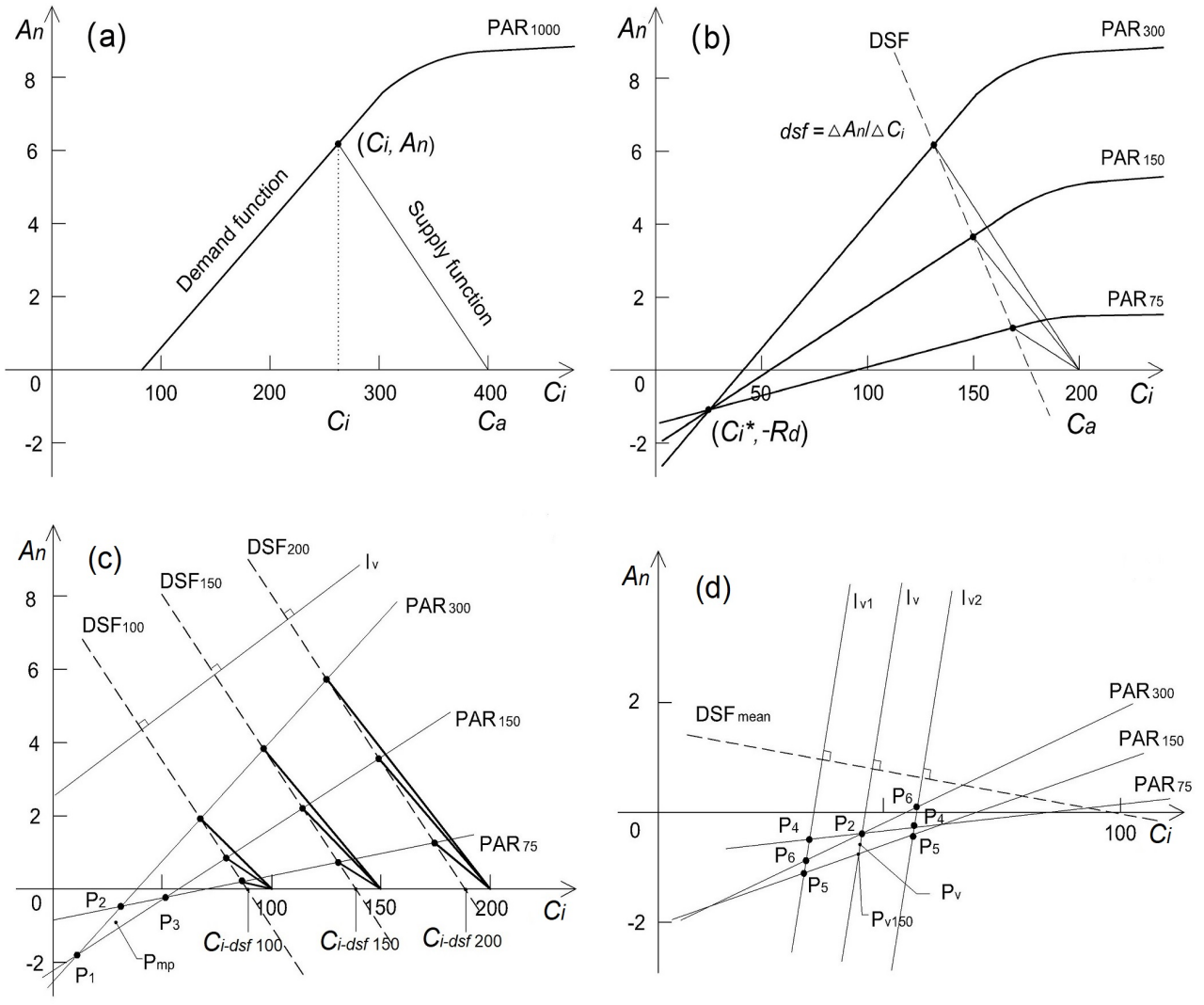

Figure 1. Demand function and Supply function of photosynthesis in A/C_i curve modified from Figure 9.7. in "Photosynthesis in silico: Understanding complexity from molecules to ecosystems" [20] and **Figure 1(b)** by Duursma [10] (a). The dark solid line indicates the "demand function" (initial part of A/C_i) the dependence of A_n on C_i, and the solid line represents the "supply function" describing the CO_2 diffusion from ambient (C_a) to intercellular spaces (C_i). The intersection (C_i, A_n) of the demand and supply curves of photosynthesis means the steady state of these two functions is equal. The intersections of demand and supply curves at 75, 150, and 300 μmol·m^{-2}·s^{-1} PARs and at 200 μmol·mol^{-1} C_a (part of the Laisk dataset) can fit into a regression line named DSF (DSF, Demand-Supply Function regression line in (b)). The slope of DSF is $\Delta A_n/\Delta C_i$ (*dsf*). Diagram of the common Laisk method (generated from a single set of measurements on the *Populus balsamifera* L., see **Table S1**) (c). P_1, P_2, P_3 are the intersecting points between PAR_{300} and PAR_{150}, PAR_{300} and PAR_{75}, PAR_{150} and PAR_{75}, and point P_{mp} is the average of P_1, P_2, P_3; Dashed lines DSF_{100}, DSF_{150}, and DSF_{200} are produced by connecting the C_i points onPAR_{75}, PAR_{150}, and PAR_{300} lines for three ambient CO_2 concentrations: 100, 150, and 200 μmol·mol^{-1}; $C_{i\text{-}dsf100}$, $C_{i\text{-}dsf150}$ and $C_{i\text{-}dsf200}$ are the x-axis intercept of DSF_{100}, DSF_{150}, and DSF_{200}, respectively; Line I_v is the proposed auxiliary line perpendicular to the mean line of DSF_{100}, DSF_{150}, and DSF_{200}. (d). Schematic diagram of using the lines in (c) and the reduction to apagoge method to derive point P_v for estimating C_i^* and $-R_d$. Line DSF_{mean} (dashed) represents the average of DSF_{100}, DSF_{150}, and DSF_{200} in (c). It is assumed that line I_v passes point P_2 (*i.e.*, the intersecting point of A/C_i lines with the highest and lowest PAR) and intersects with line PAR_{150} at point P_{v150}; P_v is the midpoint of line segment P_2-P_{v150}. Whether I_v is parallel shifted to the left (I_{v1}) or right (I_{v2}), the sum of line segments formed by the intersections of I_v and three A/C_i will increase. Therefore, the line I_v passing through P_2 intersects the PAR_{150} (the middle PAR in the Laisk measurement) at point P_{v150}, and the midpoint (P_v) of the P_2P_{v150} may be more representative of the point (C_i^*, $-R_d$). The shape of lines in (d) is more realistic relationships between different lines as shown in (c). Please see **Table 1** for other explanations.

RuBP regeneration [30] [31]. At present, g_s and C_i/C_a are used to assess the limitation of CO_2 diffusion to photosynthesis. However, these parameters are very sensitive to changes in by environmental conditions and therefore highly variable [10]. A proper evaluation of environmental effects on the demand and supply functions of photosynthesis, particularly those associated with climate change, will provide insightful information and useful data for ecological and photosynthesis models based on the biochemical and CO_2 diffusion algorithms of photosynthesis. However, there is a lack of such information in the literature. The coordination between the demand and supply functions of photosynthesis likely reflects the intrinsic characteristics of plant adaptation to the environment. Based on the measurement of Laisk dataset, We studied the regression lines (defined as the Demand-Supply Function, or DSF) connecting the intersections of the Demand Function and Supply Function of photosynthesis at different PAR under the same CO_2 concentration of leaf surface (C_a) (Laisk data according to [32]) and examined the effect of DSF slope on C_i^* and R_d estimations and the relationship of the DSF slope with CO_2 diffusion and biochemical characteristics of photosynthesis. We proposed and tested a new method to calculate C_i^* and R_d, and a new parameter to describe the coordination between DF and SF under the co-limitation of Rubisco and RuBP regeneration.

2. Materials and Methods

2.1. Plant Materials

Three broadleaf tree species, balsam poplar (*Populus balsamifera* L.), black cottonwood(*Populus trichocarpa* Torr. & Gray), and white birch (*Betula papyrifera* Marsh.) were used for this study. White birch seeds and black cottonwood branch cuttings were collected from trees in the city of Thunder Bay (48˚42'19"N, 89˚26'01"W). Balsam poplar seeds from Kemptville (45˚02"N, 75˚39'W) were obtained from the National Tree Seed Centre in Fredericton, NB, Canada. Balsam poplar and white birth seeds were processed according to The Woody Plant Seed Manual [33] and sown in germination trays in the Lakehead University greenhouse. The cottonwood cuttings were treated with a rooting hormone (Plat Prod Stim Root #3, Plant Products Co. Ltd. Brantford, ON, CA) before being planted. The cuttings were misted continuously in a polyethylene tent during the period of root induction in the greenhouse. The seedlings and rooted cuttings were transplanted into 3.5 L plastic pots filled with peat moss and vermiculite (1:1, *v:v*). The plants were watered as needed to keep the growing medium moist and fertilized twice a week with 75 $mg \cdot L^{-1}$ of a fertilizer solution (All-Purpose, 24-8-16 N-P-K fertilizer, Plant Products Co. Ltd. Mississauga, ON, CA). The greenhouse conditions were 23/16˚C day/night temperatures, 16-hour photoperiod and 50% RH. The maximum flux density of photosynthetically active radiation at the canopy level was 500 $\mu mol \cdot m^{-2} \cdot s^{-1}$ on a sunny day. The environmental conditions were monitored and controlled using an Argus Titan System (Argus Control Systems Ltd., Surrey, BC, Canada).

2.2. Gas Exchange Measurements and Parameter Estimations

Following two months of growth, six seedlings were randomly selected from each species. The gas exchange of the 1st fully expanded leaf on the terminal shoot sample trees was measured using a PP-Systems CIRAS-3 Portable Photosynthesis System equipped with a PLC3 Universal Leaf Cuvette with automatic climate control and a built-in CFM-3 Chlorophyll Fluorescence Module (PP Systems International, Inc. Amesbury, MA, USA). The photosynthetic responses to CO_2, *i.e.*, A/C_i curves, were measured between 9:00 and 16:00. The Laisk script measurements were taken at 200, 150, 100, and 50 μmol·mol^{-1} CO_2 concentration (C_a) and 300, 150, and 75 μmol·m^{-2}·s^{-1} PAR. Subsequently, full photosynthetic CO_2 response curves (A/C_i curves) were measured at 400, 300, 200, 150, 100, 50, 400, 600, 800, 1000, and 1200 μmol·mol^{-1} CO_2 and 1000 μmol·m^{-2}·s^{-1} PAR. The apparent quantum yield was derived from measurements taken at 400 μmol·mol^{-1} CO_2 and 50, 100, 150, 200, 250 μmol·m^{-2}·s^{-1} PAR; the slope of the A-C_i response was derived from light response curves ($\Delta A/\Delta C_{i\text{-}lr}$, **Figure 1(c)**). All the measurements were made on the same leaf blade.

The point P_v (novel vertical line method in 2.4 section) and P_{mp} (conventional average midpoint method in 2.5 section) of the Laisk method (**Figure 1(c)**) were estimated first and then used to calculate R_d and C_i^* (**Figure 1(b)**). The variable J method [34] was used to calculate g_m, where the electron transport (J) was calculated from chlorophyll fluorescence according to Momayyezi's protocol and Γ^* was assumed to equal to C_i^* [35]. The chlorophyll fluorescence measurement was taken using the built-in CFM-3 model in the PP Systems CIRAS-3 system.

The A/C_i data were analyzed using the Plantecophysfitaci function of the R package to produce the maximum rate of ribulose-1,5-bisphosphate (RuBP) carboxylation (V_{cmax}, μmol·m^{-2}·s^{-1}), the maximum rate of photosynthetic electron transport (J_{max}, μmol·m^{-2}·s^{-1}) [10]. The initial slope of A/C_i was recorded as the maximum apparent carboxylation efficiency (ACE = $\Delta A/\Delta C_i$).

2.3. Demand-Supply Functions (DSF)

Figure 1(c) is the Laisk schematic diagram based on actual measurements (**Table S1**). The three A/C_i lines PAR_{300}, PAR_{150}, and PAR_{75} (solid line in **Figure 1(c)**) are the initial linear part of the Demand Functions (DF) at 300, 150 and 75 μmol·m^{-2}·s^{-1} photosynthetically active radiation (PAR) flux density, respectively; the bold lines are the Supply Functions (SF) at three different ambient CO_2 concentration (C_a) of 100, 150 and 200 μmol·mol^{-1}, the slope of which represents the rate of CO_2 diffusion from leaf surface (C_a) through stomates into the intercellular space (C_i). The three intersecting points of the three supply functions for the same C_a with their corresponding demand functions measured at the three PARs fall on a straight line which we define as the Demand-Supply Function (DSF) (the three dashed lines, DSF_{200}, DSF_{150} and DSF_{100} in **Figure 1(c)**). The X-intercepts of the three DSFs are designated by their corresponding C_a as $C_{i\text{-}dsf100}$, $C_{i\text{-}dsf150}$ and

$C_{i\text{-}dsf200}$ (Figure 1(c)). The purpose of this study was to explore the characteristics and physiological significance of the Demand-Supply Functions.

2.4. Novel Vertical Line Method for Determining C_i^* and R_d

The Laisk method assumes that the initial part of three A/C_i curves measured under three unsaturated PAR flux densities will intersect at a common point (C_i^*, $-R_d$), where C_i^* represents the CO_2 compensation point at intercellular CO_2 concentration and R_d represents daytime respiration rate in absence of photorespiration. The method is based on FvCB biochemical model of photosynthesis as $A = V_c(C_c - \Gamma^*)/C_c - R_d$. Where A is the net rate of CO_2 assimilation, V_c represents the Rubisco carboxylation rate, C_c represents CO_2 concentration in the chloroplast, Γ^* is chloroplast CO_2 compensation point [13] [36]. When C_c equals Γ^*, A equals $-R_d$. Here we assume that the g_m is infinite as the Laisk method only provides C_i values but not C_c [37]. In reality, however, the three A/C_i lines rarely intersect at a single point. Instead, there are generally three pairwise intersections that form an obtuse triangle ($P_1P_2P_3$, Figure 1(c)). The conventional protocol uses the average of the three intersecting points (point P_{mp} in Figure 1(c)) to determine Ci^* and $-R_d$ [32]. But the three lines have different weights in terms of slope because of the multiple resistances to CO_2 diffusion, enzyme variables [22]. Furthermore, measurement noises can magnify the separation of the intersecting points when the differences in slope between the three lines are small.

The Demand-Supply Functions (DSF) for different C_a that we derived have similar slopes (DSF_{100}, DSF_{150}, and DSF_{200} in Figure 1(c), to be explained later) and can be used to estimate C_i^* and R_d. We proposed to use a line perpendicular to the line with the average slope (DSF_{mean} in Figure 1(d)) of the three DSFs (*i.e.*, l_v in Figure 1(c), Figure 1(d)) as an auxiliary line for estimating C_i^* and R_d. This line has a negative slope reciprocal to the average slope of DSFs and an unknown intercept. In theory, line l_v is also the initial section of an A/C_i curve (demand function) at a certain PAR, similar to PAR_{300}, PAR_{150}, and PAR_{75} (initial section of A/C_i curves measured at 300, 150, 75 μmol·m^{-2}·s^{-1} PAR, respectively, in Figure 1(c)). l_v is supposed to go through the intersection point (C_i^*, $-R_d$) that all A/C_i curves are theoretically supposed to intersect each other regardless of PAR under which the A/C_i curves are measured.

We use the reduction to absurdity by introducing the vertical line (l_v) from Laisk dataset and developed a novel vertical line method (VL) to calculate the point (C_i^*, $-R_d$). Based on the above description, it's assumed that that line l_v should pass through point P_2 that the intersection of two A/C_i with the biggest difference in PAR (PAR75 and PAR300, Figure 1(d)). A parallel shift of l_v to the left (l_{v1}) or right (l_{v2}) will increase the total length of line segments of P_4P_5, P_4P_6, P_5P_6 which are formed by the intersections of l_v and three A/Ci curves, because the total length of P_4P_6 and P_5P_6 is always greater than the length of P_2P_{v150} (Figure 1(d)). According to the FvCB model, these intersections theoretically

should converge, when the sum of the distances among the three intersecting points will be minimal and thus the position of line l_v is determined. Therefore, after passing the intersecting point P_2 between PAR_{300} and PAR_{75}, line l_v will intersect PAR_{150} at point P_{v150}, and the midpoint (P_v) of line P_2P_{v150} will be at or near the theoretical converging point (C_i^*, $-R_d$).

2.5. Comparison of Three Methods for C_i^*, R_d and g_m Estimation

In addition to the conventional average midpoint method (MP), Walker and Ort [38] proposed a slope-intercept method (SI) for Laisk data analysis. The slope-intercept method treats the slope and intercept of each A/C_i line (initial part of A/C_i curve) as a point (slope, intercept), and the points from multiple A/C_i lines produce a new regression the slope of which equals to $-C_i^*$ and the y-intercept of which gives R_d. First, we compared the estimates of C_i^* and R_d from the Laisk data set using three methods, *i.e.*, conventional average midpoint method, slope-intercept method and our novel vertical line method, and used the estimated C_i^* and R_d to estimate g_m. Secondly, C_i^* and R_d estimates using Walker's data (**Table S2**) were also produced and compared among the three methods; but we only used the lower three (50, 130, 240 $mmol \cdot m^{-2} \cdot s^{-1}$) of the five PARs because the average midpoint method and the vertical line method can only use for three PARs, and the lower three PARs are more suitable for meeting the sub-saturated light intensity requirement of the Laisk method.

2.6. Assay of Carbonic Anhydrase Activity

The assay of the carbonic anhydrase activity (CAU) was based on the bromothymol blue colorimetry described by Wilbur [39]. 0.2 g leaf blade was ground in 1 ml of 40 mM potassium phosphate buffer (pH = 8.3) using a mortar and pestle on ice. The homogenate was centrifuged for 10 min at 5000 g and 4˚C, 20 μl of the supernatant was added to 1 ml of the buffer solution containing 20 $mg \cdot L^{-1}$ bromothymol blue as a pH indicator. 1 ml CO_2-saturated water of 4˚C was then added and the time (as T) that it took for the Ph of the reaction system to change from 8.3 to 6.3 was recorded. 20 μL buffer solution only was used as control and the time of pH change from 8.3 to 6.3 after adding 1 ml CO_2-saturated water was recorded as T0. The carbonic anhydrase activity was calculated as CA (EU) = 10 × (T0 ÷ T − 1).

2.7. Statistical Analysis

The differences in the parameters of the supply and demand function (*dsf*) among different species were tested using one-way ANOVA. The effects of Lasik calculation methods and species on photosynthetic parameters were tested using two-way ANOVA. Tukey-HSD Post-hoc comparisons were conducted when ANOVA showed a significant effect. Pearson correlation analysis and linear regression were performed to examine the relationships between parameter values estimated from the P_v method and those from the other methods. All the analys-

es were conducted using R 4.0.4. Principal component analysis (PCA) was applied to photosynthetic parameters using the PCA function from the FactoMineR package.

3. Results

3.1. Characteristics of DSF: Slope and Intercept

The significant differences in the slope of the Demand-Supply Function (DSF) indicated species specificity (Table S3): the I_v slope was significantly smaller in black cottonwood than in balsam poplar and white birch (Figure 2(a)); however,

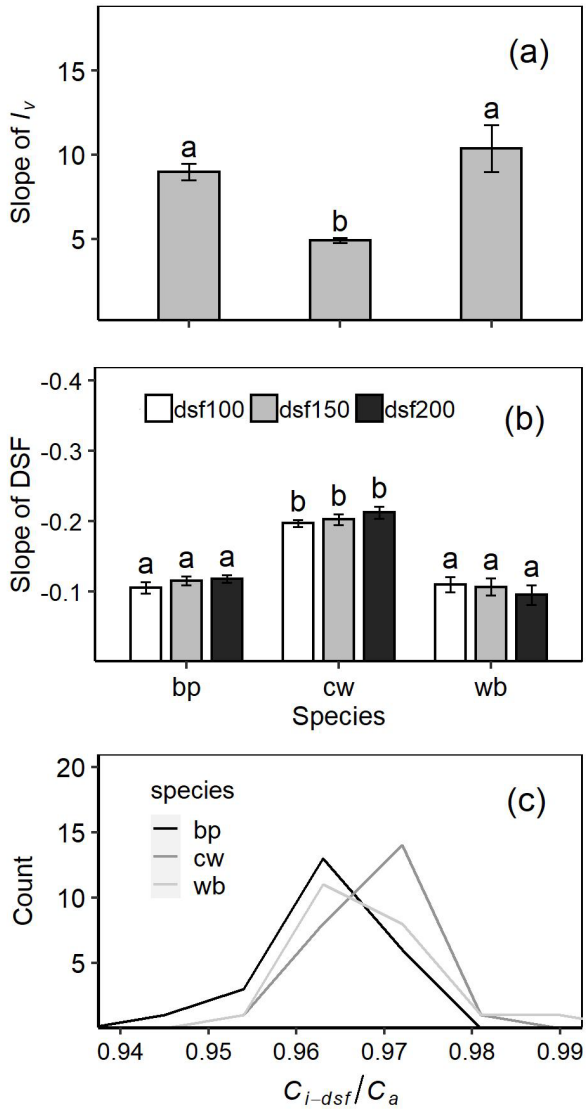

Figure 2. (a) Variation in the slope of the vertical line (I_v) among balsam poplar (bp), black cottonwood (cw) and white birch (wb); (b) Variation in the slope of Demand-Supply Function (*dsf*) with measurement C_a (100, 150, 200 μmol·m^{-2}·s^{-1}) and species; (c) Frequency distribution of DSF x-axis intercept ($C_{i\text{-}dsf}$) title to C_a ratio. Means (±SE, n = 6) with different letters in (a) and (b) were significantly different from each other ($p \leq 0.05$). Please see Table 1 for other explanations.

the trend for the slope of DSF lines was the opposite, *i.e.*, it was significantly greater in the cottonwood than in balsam poplar and white birch (Figure 2(b)). The DSF slopes of the same species for the ambient CO_2 concentration (C_a, from 100 to 200 μmol·mol^{-1}) were not significantly different from each other, suggesting that the DSF lines were approximately parallel to each other (Figure 2(b)). The coefficient of variation in DSF slope and l_v slope was much greater in white birch than the other two tree species (Table 2). The ratio of $C_{i\text{-}dsf}$ (DSF intercept on the X-axis) to C_a ($C_{i\text{-}dsf}/C_a$) in the three species was in a narrow range of 0.96 to 0.97 (Figure 2(c)). This suggests that for a given C_a, the X-axis intercept of the fitting line of the Demand-Supply Function was relatively constant.

3.2. Relationship between DSF Slope and C_i/C_a to g_s and C_a

The slope of the Demand-Supply Function (*dsf*) was inversely related to stomatal conductance (g_s) and leaf surface CO_2 concentration (C_a) and the relationship varied with species (Figure 3(a) and Figure 3(b)): balsam poplar and white birch had similar trends and had much steeper DSF slopes and smaller stomatal conductance than black cottonwood, and *dsf* had a strong correlation with and g_s (Figure 3(a)) but a weak correlation with C_a (except white birch) (Figure 3(b)). No significant correlation was observed between C_i/C_a and g_s (Figure 3(c)). C_i/C_a declined with increases in C_a, however, the relationship was not obviously different between the three species (Figure 3(d)).

3.3. Relationship between *dsf* and Photosynthetic Parameters

The multivariate relationships between photosynthetic parameters were summarized using two principal components (PCA, Figure 4). *dsf* and $\Delta A/\Delta C_{i\text{-}lrc}$

Table 2. Coefficient of variation (CV) of R_d and C_i^* estimates using the conventional average mid-point method (MP), slope-intercept method (SI) and vertical line method (VL) as well as CV for the slopes of l_v, *dsf*100, *dsf*150, and *dsf*200. See Table 1 for other explanations.

Parameters	Methods	CV		
		bp	cw	wb
R_d	MP	7.9%	4.3%	47.9%
R_d	SI	7.5%	3.4%	6.8%
R_d	VL	6.0%	3.5%	9.9%
C_i^*	MP	10.2%	9.1%	25.0%
C_i^*	SI	10.6%	8.0%	10.7%
C_i^*	VL	9.6%	7.2%	9.9%
l_v slope		13.6%	7.5%	32.9%
*dsf*100 slope		18.4%	6.3%	23.5%
*dsf*150 slope		14.3%	9.1%	28.3%
*dsf*200 slope		11.3%	9.9%	36.2%

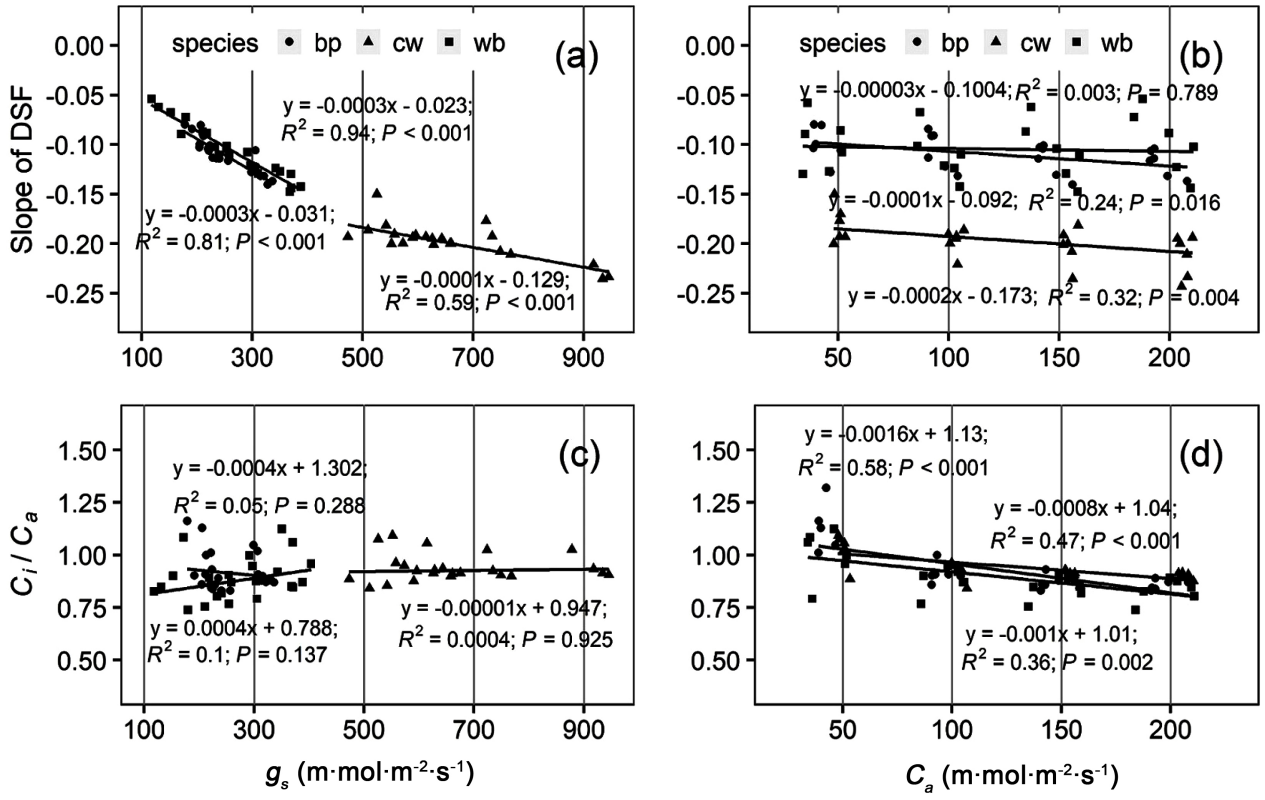

Figure 3. Relationships of DSF slope to stomatal conductance (g_s) (a) and C_a (b) and relationships of C_i/C_a ratio to g_s (c) and C_a (d). The same column or row shares axis labels and units. Please see Table 1 for other explanations.

clustered on the left side of principal component 1 (PC1) while ACE and AQY grouped on the right side, indicating that there might be negative correlations between the two groups (Figure 4). The differences in these four parameters in the three tree species were similar to those in PCA (Table S4 & Figure 4) and there were similarities within the group (*dsf* and $\Delta A/\Delta C_{i\text{-}lrc}$, ACE and AQY) while opposite variations between the groups (Figure 4 and Figure 5).

An obvious phenomenon was that *dsf* and $\Delta A/\Delta C_{i\text{-}lrc}$ almost overlapped in PCA (Figure 4), indicating a close relationship between them. ANOVA analysis verified that *dsf* and $\Delta A/\Delta C_{i\text{-}lrc}$ (the values of $\Delta A/\Delta C_i$ from different PARs) had no significant difference between different C_a but there were differences among species (Table S5), suggesting that *dsf* and $\Delta A/\Delta C_{i\text{-}lrc}$ might be species-specific and independent of the measurement conditions (PARs and C_a).

3.4. C_i^*, R_d and g_m Estimates

C_i^* and R_d estimates from our new vertical line method (VL) were not significantly different from those estimated using the conventional average midpoint method (MP) and slope-intercept method (SI) for all three tree species (Table S6 and Figure 6(a), Figure 6(b)). However, white birch had significantly lower R_d than black cottonwood and balsam poplar and the variation and coefficient of variation in R_d were much greater for the combination of the MP method and

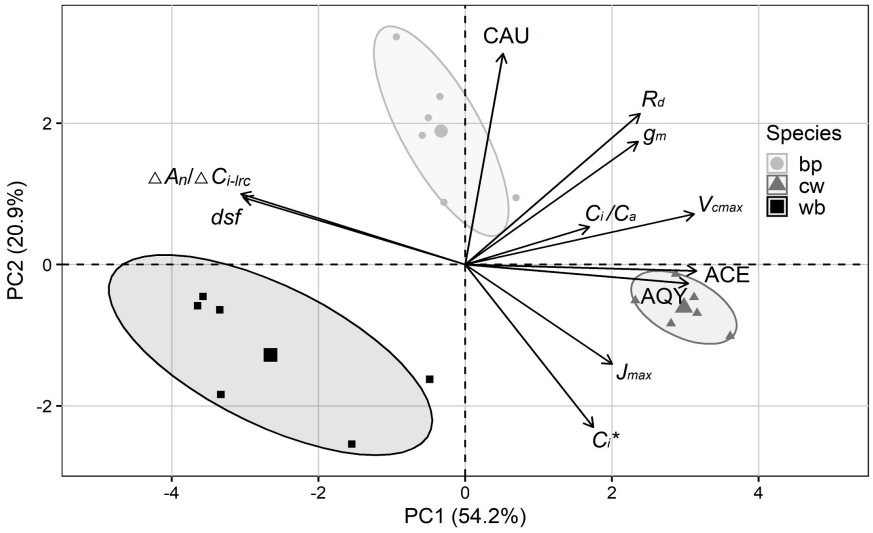

Figure 4. Principal Component Analysis (PCA) on balsam poplar (bp), black cottonwood (cw) and white birch (wb) by CAU (carbonic anhydrase activity), R_d (daytime respiration), g_m (mesophyll con-ductance), C_i/C_a ratio, V_{cmax} (maximum rate of ribulose-1,5-bisphosphate carboxylation), ACE (apparent carboxylation efficiency), AQY (apparent quantum yield), J_{max} (maximum rate of photosynthetic electron transport rate), C_i^* (intercellular CO_2 compensation point), *dsf* (DSF slope = $\Delta A_n/\Delta C_i$) and $\Delta A_n/\Delta C_{i\text{-}lrc}$ (slope of A_n vs C_i under light response curve). Please see Table 1 for other explanations.

birch than the other combinations (Table 2 & Figure 6(a)). There was no significant difference in C_i^* among the three species, but the variation and coefficient of variation in C_i^* were much larger for the combination of white birch and the MP method (Table 2 & Figure 6(b)). g_m estimation was influenced by species and the method of C_i^* and R_d estimation (Table S6). White birch had significantly lower g_m than in the other two species (Figure 6(c)), and the slope-intercept method produced significantly greater g_m estimation than the MP method and vertical line method (Figure 6(d)). The g_m calculated by the MP method was slightly smaller than that calculated by the VL method, but the difference was not statistically significant (Figure 6(d)).

Using the three lower PAR curves of Walker's data, the C_i^* and R_d estimates using the three methods were not significantly different from each other and the values from our vertical line method generally fell between those of the other two methods (Table S7). However, the slope-intercept method produced much greater R_d estimates when using 5 PAR curves (0.63) than using 3 curves (0.51) or the other two methods (0.54 and 0.52) (Table S7).

4. Discussion

4.1. Physiological Characteristics of the Demand-Supply Function

The intersecting points of supply functions and demand functions were estimated using the measurements taken under three different PARs but the same C_a and formed a straight line (DSF). The slope of DSF (*dsf*, $dsf = \Delta A_n/\Delta C_b$, Figure 1(b), Figure S2) represents A response to low PAR at various C_a and its

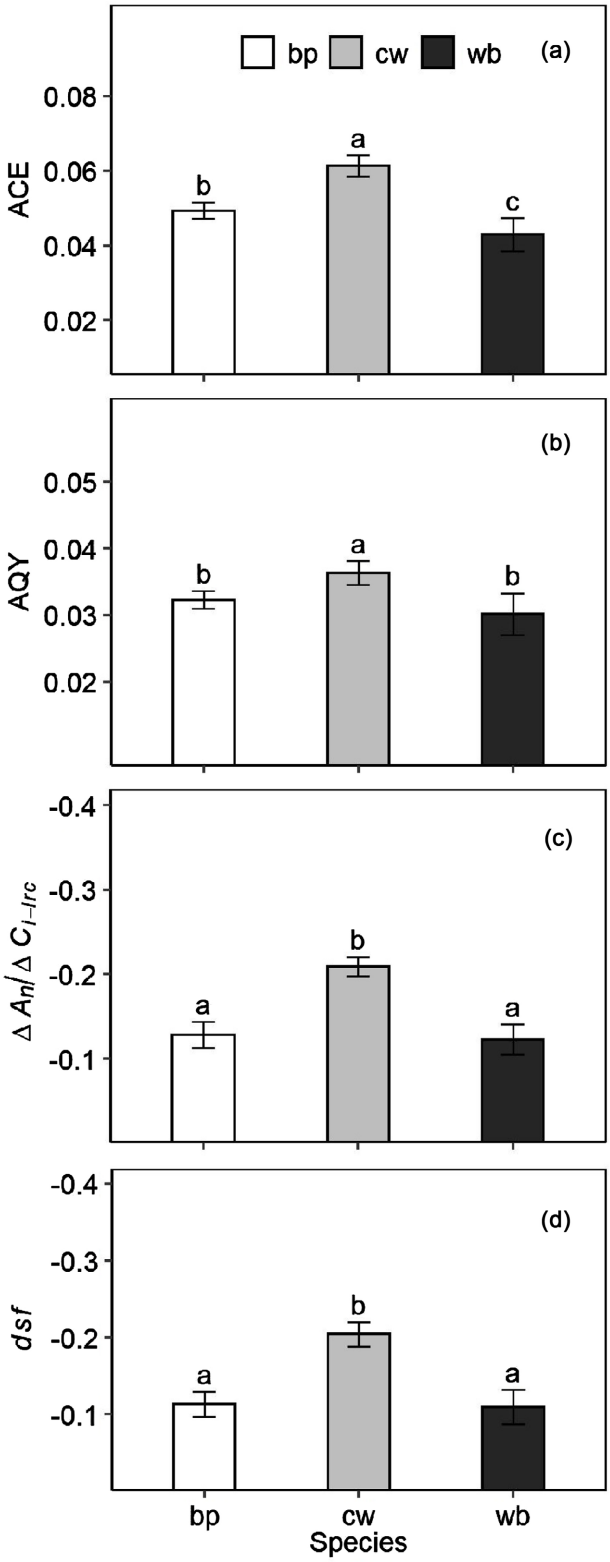

Figure 5. The estimates of ACE (apparent carboxylation efficiency (a)), AQY (apparent quantum yield, (b)), $\Delta A_n/\Delta C_{i\text{-}lrc}$ (slope of A_n vs C_i under light response curve (c)) and dsf (DSF slope, (d)) in balsam poplar (bp), black cottonwood (cw) and white birch (wb). Means (±SE, n = 6) with different letters were significantly different from each other ($p \leq 0.05$). Please see Table 1 for other explanations.

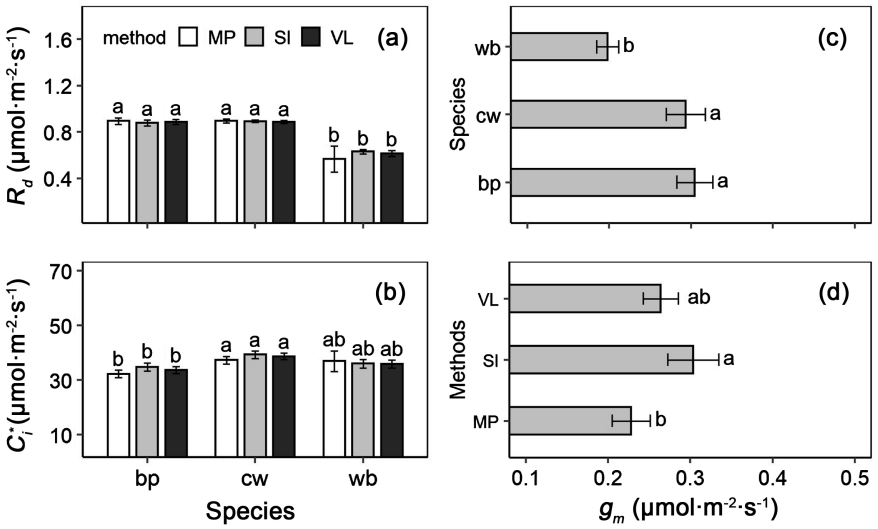

Figure 6. The estimates (mean ± SE, n = 6) of R_d (a), C_i^* (b), and g_m ((c) & (d)) in balsam poplar (bp), black cottonwood (cw) and white birch (wb) using three different methods: the conventional average midpoint method (MP), the slope-intercept method (SI) and our novel vertical line method (VL). The means with different letters are significantly different from each other ($p \leq 0.05$). Please see **Table 1** for other explanations.

absolute value represents the apparent quantum year of photosynthesis at various C_a and non-saturating PAR ($\Delta A_n/\Delta C_{i\text{-}lrc}$ in **Figure S1**). The apparent carboxylation efficiency (ACE) was derived from the initial slope of A/C_i (ACE = $\Delta A_n/\Delta C_i$, using the same algorithm as for *dsf* and $\Delta A_n/\Delta C_{i\text{-}lrc}$). Furthermore, ACE increased with increases in PAR (**Figure S3(a)**). Similarly, the apparent quantum yield (AQY) derived from the initial slope of a light response curve represents the quantum yield under a certain C_a and AQY increases with increasing C_a (**Figure S3(a)**) [30]. Many studies have identified similar patterns in ACE and AQY [38] [40] [41] [42] [43], limiting the application of ACE and AQY because they can only describe the photosynthetic characteristics under a particular measurement condition (PAR or C_a). Under dynamic environmental conditions, plants can rapidly coordinate CO_2 diffusion and biochemical fixation [44], indicating the existence of internal coordination mechanisms [45] [46].

The apparent carboxylation efficiency reflects the efficiency of assimilation of the CO_2 in the intercellular space under a certain PAR (usually saturating PAR). It is considered to be the ultimate limiting factor of CO_2 fixation and is related to the amount and activity of Rubisco [47]. Moreover, ACE increased with increases in PAR (**Figure S3(a)**), indicating that the actual intrinsic carboxylation efficiency (CEi) of a leaf was co-determined by Rubisco activity (related to V_{cmax}) and RuBP regeneration (related to J_{max}) [48]. Similarly, the initial slope of LRC (AQY) for a certain C_a increased with increases in C_a (**Figure S3(b)**). The intrinsic quantum yield (QYi) of a leaf may be affected by both Rubisco activity and RuBP regeneration [31]. V_{cmax} and J_{max} (as indicators of photosynthetic capacity) might excert their effects through carboxylation efficiency and quantum yield [25]. These were partially explained by PCA results where ACE and AQY were

grouped in the middle region of V_{cmax} and J_{max}. However, other studies have shown that V_{cmax} and J_{max} are independent of g_s and CO_2 diffusion [48]. To sum up, *dsf* or $\Delta A_n/\Delta C_{i\text{-}lrc}$ may provide a link between CO_2 diffusion and biochemical characteristics of photosynthesis because of its close relationships with g_s, ACE and AQY.

The values of Laisk measurements are co-limited by Rubisco and RuBP regeneration. The Rubisco restriction is reflected in the linear or initial portion of an A/C_i curve and RuBP regeneration restriction prevents the lines with different PAR from overlapping [49]. Hence, *dsf* (or $\Delta A_n/\Delta C_{i\text{-}lrc}$) probably acts as an internal coordination mechanism between CO_2 diffusion and fixation in photosynthesis when PAR and C_a both change simultaneously [50]. Rubisco limitation and RuBP regeneration limitation often co-exist in the nature, especially under fluctuating light and drought conditions (may cause C_i decrease) [51]. Therefore, results derived from a normal A/C_i (ACE, V_{cmax} and J_{max}) and LRC (AQY) may not be suitable to explain photosynthesis at these conditions.

Another feature of *dsf* or $\Delta A_n/\Delta C_{i\text{-}lrc}$ is that it is independent of gas exchange measurement conditions (lower PAR and C_a). The *dsf* has little dependence on C_a since the Michaelis–Menten constants for the carboxylase (K_c) are relatively large [29] [52], which may explain why DSF from different C_a were almost parallel to each other and why there was no significant difference between *dsf* and $\Delta A_n/\Delta C_{i\text{-}lrc}$. This property allows the use of *dsf* or $\Delta A_n/\Delta C_{i\text{-}lrc}$ to link CO_2 supply and biochemical demand of photosynthesis when Rubisco and RuBP regeneration are co-limiting.

4.2. Demand-Supply Function vs C_i/C_a

The supply function reflects the diffusion of CO_2 while the demand function reflects the photochemical and biochemical processes of CO_2 assimilation as a function of intercellular CO_2 concentration (C_i) [20]. C_i acts as a CO_2 pool connecting upstream and downstream, which regulates the supply-demand relationship of photosynthesis to a certain extent [53]. Our results showed that C_i/C_a was not closely related to g_s within the range of C_a used in this study although it decreased with decreases in C_a to some extent while no significant differences between in species. Woody plants usually adopt a dynamic leaf gas-exchange strategy and do not maintain a constant value of C_i/C_a [9]. Therefore, C_i/C_a was not suitable to describing coordination between CO_2 diffusion and photosynthetic biochemistry under the Laisk measurement protocol in the three species. However, the slope of the Demand-Supply function was closely related to g_s, and different between the species and thus may better reflect the response of photosynthesis to stomatal conductance.

4.3. The Vertical Line Method Improves C_i^* and R_d Estimation

There are concerns about the validity of Laisk method which is widely used to estimate R_d [23]. Our results demonstrate that the novel vertical line method

produced more robust estimates of C_i^* and R_d than the conventional average midpoint method, especially in white birch. Although the theoretical basis of the Laisk method is the FvCB model, the R_d estimate using the original Laisk method (Laisk 1977) is compromised because decreasing light reduces C_i^* which in turn affects the estimate of R_d [36]. The Laisk method uses the initial portion of A/C_i curves under several sub-saturation light intensities. However, it is unknown whether photosynthesis is limited by Rubisco activities or by RuBP regeneration under such measurement conditions. Those partial A/C_i curves theoretically should intersect at a single point defined by (C_i^*, $-R_d$), but different curves have different weights on the determination of the intersecting point [22]. The different A/C_i curves measured in the Laisk Method tend to have similar slopes and a great degree of overlapping. Consequently, the determination of the intersection point and thus C_i^* and R_d estimation are more vulnerable to instrument and operation errors [38].

The conventional average midpoint method directly averages the coordinate values of the pairwise intersecting points of three A/C_i curves and therefore is also prone to errors if the differences in slopes are small [38]. Mean values of C_i^* and R_d fluctuate greatly (higher coefficient of variation) when calculated by the average midpoint method in white birch, leading to difficulties for the application of the Laisk method. Our results show that the coefficient of variation of l_v slope (from the average DSF slope) of white birch was significantly larger than those of the other two species, and the DSF showed a slightly increasing trend with increases in C_a *and was lower* in black cottonwood and balsam poplar, suggesting that the poor performance of the Laisk method (*i.e.*, failure to intersect at one point or the intersection was not in the fourth quadrant) in white birch may be related to the coordination of supply and demand functions. The vertical line method produced more robust estimates of C_i^* and R_d than the average midpoint method, possibly because the slope of the auxiliary line l_v was much larger than those of the initial A/C_i lines in the conventional Laisk method. Deeper slopes generally produce more stable and reliable determinations of the intersecting point [54].

5. Conclusion

Our results show that the demand-supply function (DSF) concept and the auxiliary line approach that we developed in this study represent a significant enhancement to the conventional Laisk method. The slope of DSF was essentially $\Delta A_n/\Delta C_{i\text{-}lrc}$ measured by LRC. Using an auxiliary line perpendicular to DSF can improve the stability of Laisk method for estimating C_i^* and R_d. The *dsf* was negatively correlated with g_s, ACE, and AQY, and linked CO_2 diffusion limitation and biochemical limitation of photosynthesis. The *dsf* should be particularly useful for modeling photosynthesis under dynamic other environment conditions (particularly light) than conventional CO_2 diffusion (g_s, C_i/C_a) and biochemical (V_{cmax}, J_{max}, ACE, AQY) photosynthesis models alone. Our results sug-

gest that *dsf* (or $\Delta A_n/\Delta C_{i\text{-}lrc}$) may be species specific. Since it was independent of measurement environment conditions (PAR and C_a), DSF can be used to characterize the intrinsic coordination between CO_2 diffusion and biochemical carbon fixation in photosynthesis. The ability of photosynthesis and ecological models to consider dynamic, non-saturating light conditions should become more important in the future for predicting plant response to climate change because such an ability will provide more realistic estimates of the dynamic activities of photosynthesis associated with dynamic environmental conditions. Environmental conditions will likely be more dynamic in the future [18].

Acknowledgements

We want to thank Ms. Keri Pidgen, Greenhouse Manager of Lakehead University for her logistic support and other operational assistance during the experiments. We also thank the National Tree Seed Centre of Canada for providing balsam poplar seeds.

Supplementary Materials

Additional supporting information may be found online in the Supporting Information section at the end of the article.

Conflicts of Interest

The authors declare no conflicts of interest regarding the publication of this paper.

References

[1] Wu, J.-T., Wang, L., Zhao, L., Huang, X.-C. and Ma, F. (2020) Arbuscular Mycorrhizal Fungi Effect Growth and Photosynthesis of *Phragmites australis* (Cav.) Trin ex. Steudel under Copper Stress. *Plant Biology*, **22**, 62-69. https://doi.org/10.1111/plb.13039

[2] Kong, R.S., Way, D.A., Henry, H.A.L. and Smith, N.G. (2022) Stomatal Conductance, Not Biochemistry, Drives Low Temperature Acclimation of Photosynthesis in *Populus balsamifera*, Regardless of Nitrogen Availability. *Plant Biology*, **24**, 766-779. https://doi.org/10.1111/plb.13428

[3] Wang, Y., Xu, S., Zhang, W., Li, Y., Wang, N., He, X. and Chen, W. (2021) Responses of Growth, Photosynthesis and Related Physiological Characteristics in Leaves of *Acer ginnala* Maxim. to Increasing Air Temperature and/or Elevated O_3. *Plant Biology*, **23**, 221-231. https://doi.org/10.1111/plb.13240

[4] Rasool, S.G., Gulzar, S., Hameed, A., Edwards, G.E., Khan, M.A. and Gul, B. (2019) Maintenance of Photosynthesis and the Antioxidant Defence Systems Have Key Roles for Survival of *Halopeplis perfoliata* (*Amaranthaceae*) in a Saline Environment. *Plant Biology*, **21**, 1167-1175. https://doi.org/10.1111/plb.13033

[5] Xu, Y., Fu, X., Sharkey, T.D., Shachar-Hill, Y. and Walker, B.J. (2021) The Metabolic Origins of Non-Photorespiratory CO_2 Release during Photosynthesis: A Metabolic Flux Analysis. *Plant Physiology*, **186**, 297-314. https://doi.org/10.1093/plphys/kiab076

[6] Busch, F.A. (2013) Current Methods for Estimating the Rate of Photorespiration in Leaves. *Plant Biology*, **15**, 648-655. https://doi.org/10.1111/j.1438-8677.2012.00694.x

[7] Buckley, T.N., Vice, H. and Adams, M.A. (2017) The Kok Effect in *Vicia faba* Cannot Be Explained Solely by Changes in Chloroplastic CO_2 Concentration. *New Phytologist*, **216**, 1064-1071. https://doi.org/10.1111/nph.14775

[8] Xiong, D., Douthe, C. and Flexas, J. (2018) Differential Coordination of Stomatal Conductance, Mesophyll Con-Ductance, and Leaf Hydraulic Conductance in Response to Changing Light across Species. *Plant, Cell & Environment*, **41**, 436-450. https://doi.org/10.1111/pce.13111

[9] Voelker, S.L., Brooks, J.R., Meinzer, F.C., Anderson, R., Bader, M.K.-.-F., Battipaglia, G., Becklin, K.M., Beerling, D., Bert, D., Betancourt, J.L., Dawson, T.E., Domec, J.-C., Guyette, R.P., Körner, C., Leavitt, S.W., Linder, S., Marshall, J.D., Mildner, M., Ogée, J., Panyushkina, I., Plumpton, H.J., Pregitzer, K.S., Saurer, M., Smith, A.R., Siegwolf, R.T.W., Stambaugh, M.C., Talhelm, A.F., Tardif, J.C., Van de Water, P.K., Ward, J.K. and Wingate, L. (2016) A Dynamic Leaf Gas-Exchange Strategy Is Conserved in Woody Plants under Changing Ambient CO_2: Evidence from Carbon Isotope Discrimination in Paleo and CO_2 Enrichment Studies. *Global Change Biology*, **22**, 889-902. https://doi.org/10.1111/gcb.13102

[10] Duursma, R.A. (2015) Plantecophys—An R Package for Analysing and Modelling Leaf Gas Exchange Data. *PLOS ONE*, **10**, e0143346. https://doi.org/10.1371/journal.pone.0143346

[11] Busch, F.A. (2020) Photorespiration in the Context of Rubisco Biochemistry, CO_2 Diffusion and Metabolism. *The Plant Journal*, **101**, 919-939. https://doi.org/10.1111/tpj.14674

[12] Fernández-Marín, B., Gulías, J., Figueroa, C.M., Iñiguez, C., Clemente-Moreno, M.J., Nunes-Nesi, A., Fernie, A.R., Cavieres, L.A., Bravo, L.A., García-Plazaola, J.I. and Gago, J. (2020) How Do Vascular Plants Perform Photosynthesis in Extreme Environments? An Integrative Ecophysiological and Biochemical Story. *The Plant Journal*, **101**, 979-1000. https://doi.org/10.1111/tpj.14694

[13] Farquhar, G.D., von Caemmerer, S. and Berry, J.A. (1980) A Biochemical Model of Photosynthetic CO_2 Assimilation in Leaves of C_3 Species. *Planta*, **149**, 78-90. https://doi.org/10.1007/BF00386231

[14] Yin, X., Busch, F.A., Struik, P.C. and Sharkey, T.D. (2021) Evolution of a Biochemical Model of Steady-State Photosynthesis. *Plant, Cell & Environment*, **44**, 2811-2837. https://doi.org/10.1111/pce.14070

[15] Zhou, H., Xu, M., Pan, H. and Yu, X. (2015) Leaf-Age Effects on Temperature Responses of Photosynthesis and Respiration of an Alpine Oak, *Quercus aquifolioides*, in Southwestern China. *Tree Physiology*, **35**, 1236-1248. https://doi.org/10.1093/treephys/tpv101

[16] Edlyn, B.E., Duursma, R.A., Eamus, D., Ellsworth, D.S., Prentice, I.C., Barton, C.V.M., Crous, K.Y., De Angelis, P., Freeman, M. and Wingate, L. (2011) Reconciling the Optimal and Empirical Approaches to Modelling Stomatal Conductance. *Global Change Biology*, **7**, 2134-2144. https://doi.org/10.1111/j.1365-2486.2010.02375.x

[17] Lamba, S., Hall, M., Räntfors, M., Chaudhary, N., Linder, S., Way, D., Uddling, J and Wallin, G. (2018) Physiological Acclimation Dampens Initial Effects of Elevated Temperature and Atmospheric CO_2 Concentration in Mature Boreal Norway Spruce. *Plant, Cell & Environment*, **41**, 300-313. https://doi.org/10.1111/pce.13079

[18] Pastore, M.A., Lee, T.D., Hobbie, S.E. and Reich, P.B. (2020) Interactive Effects of Elevated CO_2, Warming, Reduced Rainfall, and Nitrogen on Leaf Gas Exchange in Five Perennial Grassland Species. *Plant, Cell & Environment*, **43**, 1862-1878. https://doi.org/10.1111/pce.13783

[19] Lambers, H., Chapin, F.S. and Pons, T.L. (2008) Plant Physiological Ecology. Springer, New York. https://doi.org/10.1007/978-0-387-78341-3

[20] Laĭsk, A.K., Nedbal, L. and Govindjee (2009) Photosynthesis in Silico: Understanding Complexity from Molecules to Ecosystems. Springer, Dordrecht. https://doi.org/10.1007/978-1-4020-9237-4

[21] Taiz, L., Zeiger, E., Møller, I.M. and Murphy, A. (2018) Plant Physiology and Development. Oxford University Press, Oxford.

[22] Walker, B.J., Skabelund, D.C., Busch, F.A. and Ort, D.R. (2016) An Improved Approach for Measuring the Impact of Multiple CO_2 Conductances on the Apparent Photorespiratory CO_2 Compensation Point through Slope-Intercept Regression. *Plant, Cell & Environment*, **39**, 1198-1203. https://doi.org/10.1111/pce.12722

[23] Tcherkez, G., Gauthier, P., Buckley, T.N., Busch, F.A., Barbour, M.M., Bruhn, D., Heskel, M.A., Gong, X.Y., Crous, K.Y., Griffin, K., Way, D., Turnbull, M., Adams, M.A., Atkin, O.K., Farquhar, G.D. and Cornic, G. (2017) Leaf Day Respiration: Low CO2 Flux but High Significance for Metabolism and Carbon Balance. *New Phytologist*, **216**, 986-1001. https://doi.org/10.1111/nph.14816

[24] Yin, X., Sun, Z., Struik, P.C. and Gu, J. (2011) Evaluating a New Method to Estimate the Rate of Leaf Respiration in the Light by Analysis of Combined Gas Exchange and Chlorophyll Fluorescence Measurements. *Journal of Experimental Botany*, **62**, 3489-3499. https://doi.org/10.1093/jxb/err038

[25] Bloomfield, K.J., Prentice, I.C., Cernusak, L.A., Eamus, D., Medlyn, B.E., Rumman, R., Wright, I.J., Boer, M.M., Cale, P., Cleverly, J., Egerton, J.J.G., Ellsworth, D.S., Evans, B.J., Hayes, L.S., Hutchinson, M.F., Liddell, M.J., Macfarlane, C., Meyer, W.S., Togashi, H.F., Wardlaw, T., Zhu, L. and Atkin, O.K. (2019) The Validity of Optimal Leaf Traits Modelled on Environmental Conditions. *New Phytologist*, **221**, 1409-1423. https://doi.org/10.1111/nph.15495

[26] Bellasio, C., Beerling, D. J., and Griffiths, H. (2016) An Excel Tool for Deriving Key Photosynthetic Parameters from Combined Gas Exchange and Chlorophyll Fluorescence: Theory and Practice. *Plant, Cell & Environment*, **39**, 1180-1197. https://doi.org/10.1111/pce.12560

[27] Green, J.K. and Keenan, T.F. (2022) The Limits of Forest Carbon Sequestration. *Science*, **376**, 692-693. https://doi.org/10.1126/science.abo6547

[28] Weber, J.A., Tenhunen, J.D. and Lange, O.L. (1985) Effects of Temperature at Constant Air Dew Point on Leaf Carboxylation Efficiency and CO_2 Compensation Point of Different Leaf Types. *Planta*, **166**, 81-88. https://doi.org/10.1007/BF00397389

[29] Teramura, A.H., Sullivan, J.H. and Ziska, L.H. (1990) Interaction of Elevated Ultraviolet-B Radiation and CO_2 on Productivity and Photosynthetic Characteristics in Wheat, Rice, and Soybean. *Plant Physiology*, **94**, 470-475. https://doi.org/10.1104/pp.94.2.470

[30] Song, X., Zhou, G., Xu, Z., Lv, X. and Wang, Y. (2016) A Self-Photoprotection Mechanism Helps *Stipa baicalensis* Adapt to Future Climate Change. *Scientific Reports*, **6**, Article No. 25839. https://doi.org/10.1038/srep25839

[31] Li, Y.-T., Li, Y., Li, Y.-N., Liang, Y., Sun, Q., Li, G., Liu, P., Zhang, Z.-S and Gao, H.-Y. (2020) Dynamic Light Caused Less Photosynthetic Suppression, Rather than More, under Nitrogen Deficit Conditions than under Sufficient Nitrogen Supply

Conditions in Soybean. *BMC Plant Biology*, **20**, Article No. 339. https://doi.org/10.1186/s12870-020-02516-y

[32] Laĭsk, A.K. (1977) Kinetics of Photosynthesis and Photorespiration of C_3 in Plants. Nauka, Moscow. (In Russia)

[33] United States Department of Agriculture (2008) The Woody Plant Seed Manual. United States Department of Agriculture, Washington DC.

[34] Harley, P.C., Loreto, F., Di Marco, G. andSharkey, T.D. (1992) Theoretical Considerations When Estimating the Mesophyll Conductance to CO_2 Flux by Analysis of the Response of Photosynthesis to CO_2. *Plant Physiology*, **98**, 1429-1436. https://doi.org/10.1104/pp.98.4.1429

[35] Momayyezi, M. and Guy, R.D. (2017) Substantial Role for Carbonic Anhydrase in Latitudinal Variation in Mesophyll Conductance of *Populus trichocarpa* Torr. & Gray. *Plant, Cell & Environment*, **40**, 138-149. https://doi.org/10.1111/pce.12851

[36] Ubierna, N., Cernusak, L.A., Holloway-Phillips, M., Busch, F.A., Cousins, A.B. and Farquhar, G.D. (2019) Critical Review: Incorporating the Arrangement of Mitochondria and Chloroplasts into Models of Photosynthesis and Carbon Isotope Discrimination. *Photosynthesis Research*, **141**, 5-31. https://doi.org/10.1007/s11120-019-00635-8

[37] Sun, Y., Gu, L., Dickinson, R.E., Pallardy, S.G., Baker, J., Cao, Y., Damatta, F.M., Dong, X., Ellsworth, D., Van Goethem, D., Jensen, A.M., Law, B.E., Loos, R., Martins, S.C.V., Norby, R.J., Warren, J., Weston, D. and Winter, K. (2014) Asymmetrical Effects of Mesophyll Conductance on Fundamental Photosynthetic Parameters and Their Relationships Estimated from Leaf Gas Exchange Measurements. *Plant, Cell & Environment*, **37**, 978-994. https://doi.org/10.1111/pce.12213

[38] Walker, B.J. and Ort, D.R. (2015) Improved Method for Measuring the Apparent CO_2 Photocompensation Point Resolves the Impact of Multiple Internal Conductances to CO_2 to Net Gas Exchange. *Plant, Cell & Environment*, **38**, 2462-2474. https://doi.org/10.1111/pce.12562

[39] Wilbur, K.M. and Anderson, N.G. (1948) Electrometric and Colorimetric Determination of Carbonic Anhydrase. *Journal of Biological Chemistry*, **176**, 147-154. https://doi.org/10.1016/S0021-9258(18)51011-5

[40] Yin, X., Niu, Y., van der Putten, P.E.L. and Struik, P.C. (2020) The Kok Effect Revisited. *New Phytologist*, **227**, 1764-1775. https://doi.org/10.1111/nph.16638

[41] Xiao, Y., Sloan, J., Hepworth, C., Osborne, C.P., Fleming, A.J., Chen, X. and Zhu, X.-G. (2021) Estimating Uncertainty: A Bayesian Approach to Modelling Photosynthesis in C_3 Leaves. *Plant, Cell & Environment*, **44**, 1436-1450. https://doi.org/10.1111/pce.13995

[42] Farquhar, G.D. and Busch, F.A. (2017) Changes in the Chloroplastic CO_2 Concentration Explain Much of the Observed Kok Effect: A Model. *New Phytologist*, **214**, 570-584. https://doi.org/10.1111/nph.14512

[43] Tholen, D., Ethier, G., Genty, B., Pepin, S. and Zhu, X.-G. (2012) Variable Mesophyll Conductance Revisited: Theoretical Background and Experimental Implications. *Plant, Cell & Environment*, **35**, 2087-2103. https://doi.org/10.1111/j.1365-3040.2012.02538.x

[44] Kaiser, E., Correa Galvis, V and Armbruster, U. (2019) Efficient Photosynthesis in Dynamic Light Environments: A Chloroplast's Perspective. *Biochemical Journal*, **476**, 2725-2741. https://doi.org/10.1042/BCJ20190134

[45] Eyland, D., van Wesemael, J., Lawson, T. and Carpentier, S. (2021) The Impact of Slow Stomatal Kinetics on Photosynthesis and Water Use Efficiency under Fluc-

tuating Light. *Plant Physiology*, **186**, 998-1012.
https://doi.org/10.1093/plphys/kiab114

[46] Garmash, E.V. (2021) Role of Mitochondrial Alternative Oxidase in the Regulation of Cellular Homeostasis during Development of Photosynthetic Function in Greening Leaves. *Plant Biology*, **23**, 221-228. https://doi.org/10.1111/plb.13217

[47] Li, Y., Gao, Y., Xu, X., Shen, Q. and Guo, S. (2009) Light-Saturated Photosynthetic Rate in High-Nitrogen Rice (*Oryza sativa* L.) Leaves Is Related to Chloroplastic CO_2 Concentration. *Journal of Experimental Botany*, **60**, 2351-2360.
https://doi.org/10.1093/jxb/erp127

[48] Silva-Pérez, V., de Faveri, J., Molero, G., Deery, D.M., Condon, A.G., Reynolds, M.P., Evans, J.R. and Furbank, R.T. (2020) Genetic Variation for Photosynthetic Capacity and Efficiency in Spring Wheat. *Journal of Experimental Botany*, **71**, 2299-2311. https://doi.org/10.1093/jxb/erz439

[49] Gu, L. and Sun, Y. (2014) Artefactual Responses of Mesophyll Conductance to CO_2 and Irradiance Estimated with the Variable *J* and Online Isotope Discrimination Methods. *Plant, Cell & Environment*, **37**, 1231-1249.
https://doi.org/10.1111/pce.12232

[50] Smith, N.G., Keenan, T.F., Colin Prentice, I., Wang, H., Wright, I.J., Niinemets, Ü., Crous, K.Y., Domingues, T.F., Guerrieri, R., Yoko Ishida, F., Kattge, J., Kruger, E.L., Maire, V., Rogers, A., Serbin, S.P., Tarvainen, L., Togashi, H.F., Townsend, P.A., Wang, M., Weerasinghe, L.K. and Zhou, S.-X. (2019) Global Photosynthetic Capacity Is Optimized to the Environment. *Ecology Letters*, **22**, 506-517.
https://doi.org/10.1111/ele.13210

[51] Henry, C., John, G.P., Pan, R., Bartlett, M.K., Fletcher, L.R., Scoffoni, C. and Sack, L. (2019) A Stomatal Safety-Efficiency Trade-off Constrains Responses to Leaf Dehydration. *Nature Communications*, **10**, Article No. 3398.
https://doi.org/10.1038/s41467-019-11006-1

[52] von Caemmerer, B.S. (2000) Biochemical Models of Leaf Photosynthesis. CSIRO Publishing, Clayton.

[53] Hanson, D.T., Stutz, S.S. and Boyer, J.S. (2016) Why Small Fluxes Matter: The Case and Approaches for Improving Measurements of Photosynthesis and (Photo) Respiration. *Journal of Experimental Botany*, **67**, 3027-3039.
https://doi.org/10.1093/jxb/erw139

[54] Way, D.A., Aspinwall, M.J., Drake, J.E., Crous, K.Y., Campany, C.E., Ghannoum, O., Tissue, D.T. and Tjoelker, M.G. (2019) Responses of Respiration in the Light to Warming in Field-Grown Trees: A Comparison of the Thermal Sensitivity of the Kok and Laisk Methods. *New Phytologist*, **222**, 132-143.
https://doi.org/10.1111/nph.15566

Supplementary Materials

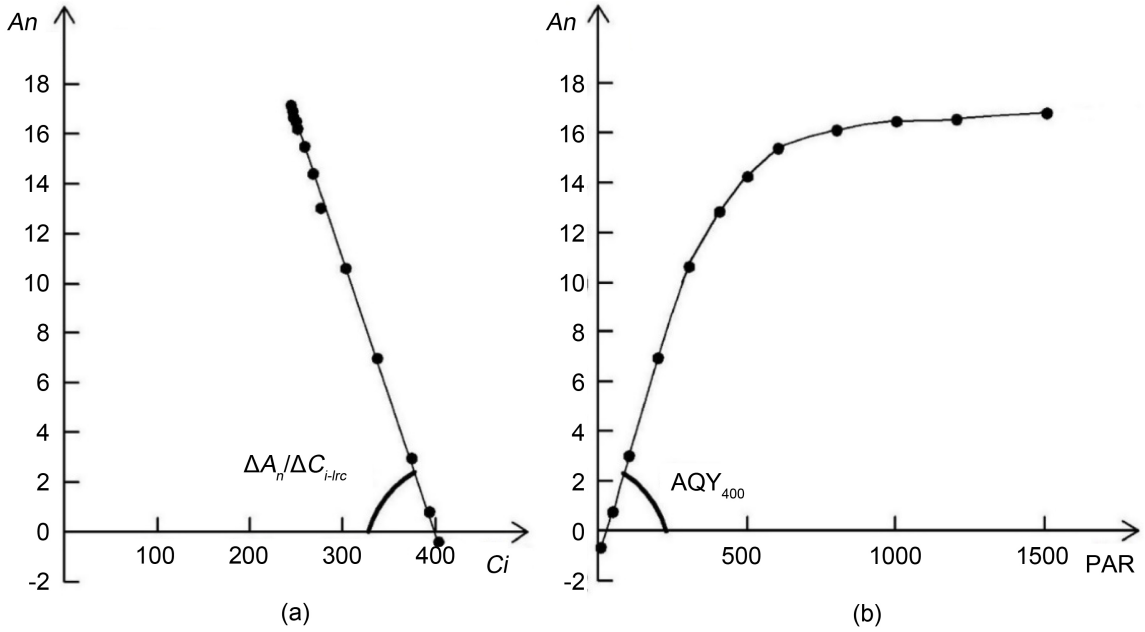

Figure S1. An example diagram of light response curve (LRC) measured at 400 μmol·mol^{-1} ambient CO_2 concentration with black cottonwood. (a): A_n vs. C_i form LRC data and the slope is $\Delta A_n/\Delta C_{i\text{-}lrc}$ (slope of A_n variation vs C_i variation under light response curve). (b): normal LRC with A_n vs. PAR and the initial slope represent apparent carboxylation efficiency (AQY) for 400 μmol·mol^{-1} of C_a.

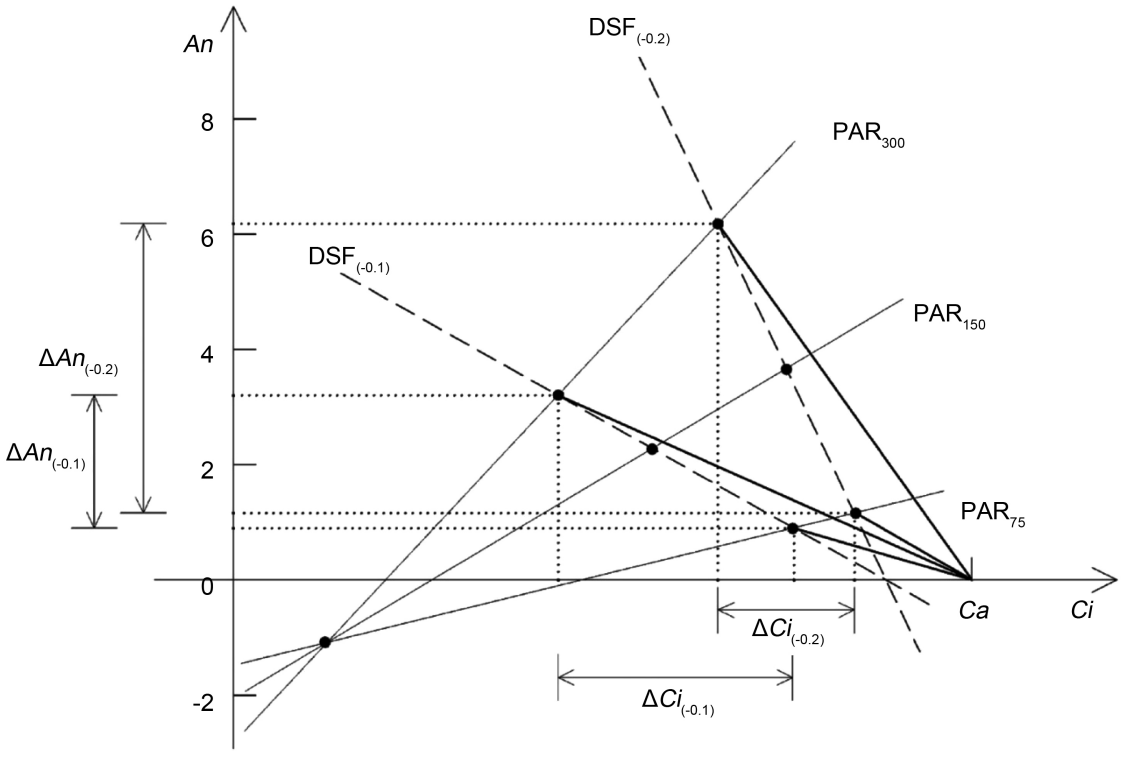

Figure S2. Schematic of demand-supply function (DSF) slope (*dsf*) change from −0.2 to −0.1 based on the measurement of an example. Slope of DSF (−0.2) = ΔA_n (−0.2)/ΔC_i (−0.2) and DSF (−0.1) = ΔA_n (−0.1)/ΔC_i (−0.1) may reflect the carboxylation efficiency of photosynthesis during the Laisk measurement (PAR from 75 μmol·m^{-2}·s^{-1} to 300 μmol·m^{-2}·s^{-1}).

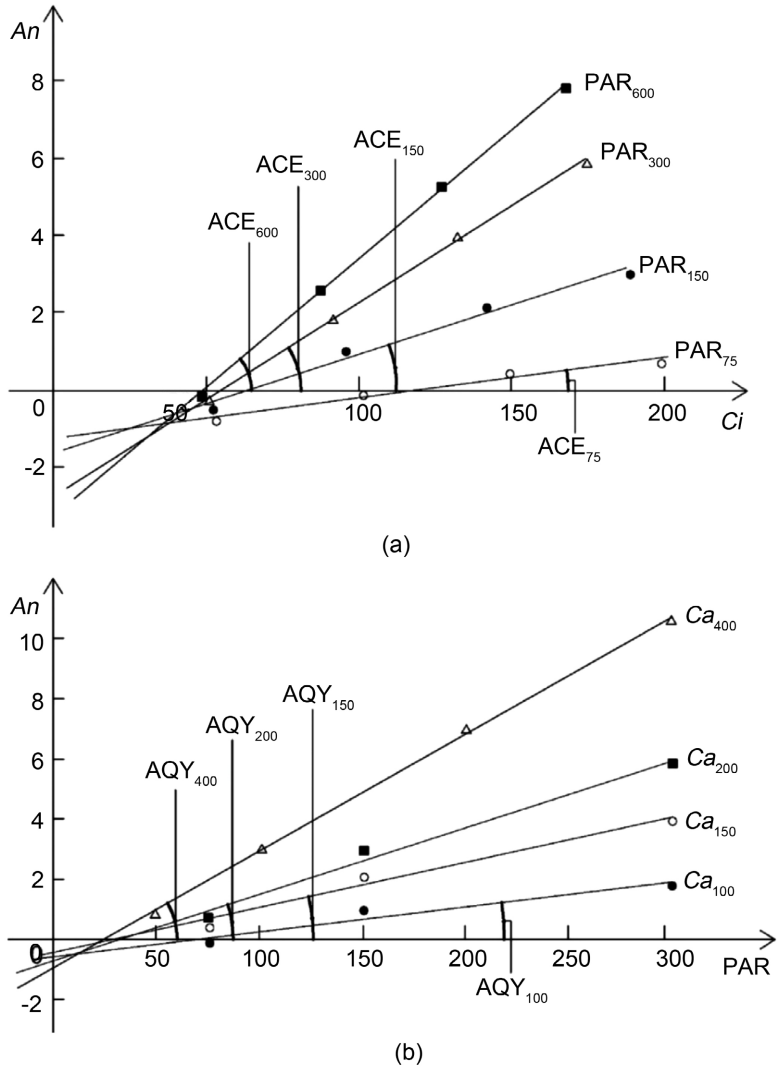

Figure S3. Diagram of A/C_i (a) and light response curve (b) on black cottonwood as an example. The apparent carboxylation efficiency (ACE) increased with the increase of PARs (a), while the apparent quantum yield (AQY) increased with the increase of C_a (b).

Table S1. Actual Laisk measurements on black cottonwood showing in **Figure 2**.

C_a	PAR	C_i	A_n
200	300	124.9	5.7
200	150	148.8	3.6
200	75	174.1	1.3
150	300	96	3.8
150	150	113.9	2.2
150	75	130.2	0.7
100	300	67.2	1.9
100	150	79	0.8
100	75	86.2	0.2

Table S2. A Laisk dataset from Walker's Supplemental 5 in "An improved approach for measuring the impact of multiple CO_2 conductance on the apparent photorespiratory CO_2 compensation point through slope-intercept regression." The unit of C_i was converted from Pa to μmol·mol^{-1}.

PAR1 (800)		PAR2 (420)		PAR3 (240)		PAR4 (130)		PAR5 (50)	
A_n	C_i	A_n	C_i	A_n	C_i	A_n	C_i	A_n	C_i
4.03	91.68	3.58	95.66	2.84	99.33	2.08	103.75	0.678	112.04
2.47	72.62	2.18	74.65	1.83	76.69	1.24	79.84	0.35	85.03
1.44	59.65	1.24	60.79	1	62.2	0.67	64.08	0.05	67.71
0.34	46.64	0.24	47.10	0.1	48.03	−0.07	48.97	−0.3	50.53
−0.81	33.76	−0.86	34.16	−0.79	33.75	−0.78	34.24	−0.78	34.19

Table S3. ANOVA *P*-values for the effects of species and C_a (leaf surface CO_2 concentration) on DSF (Demand-Supply Function) slope and vertical line (I_v) slope. The species were balsam poplar, black cottonwood and white birch. DSFs were for 100, 150 and 200 μmol·m^{-2}·s^{-1} C_a.

Factor	DSF slope	Vertical line slope
Species	**$P < 0.001$**	**0.001**
C_a	0.817	NA
Species X C_a	0.491	NA

Table S4. ANOVA *P*-values for the effects of species on ACE, $\Delta A_n/\Delta C_{i\text{-}lrc}$, AQY, and *dsf*. See **Figure 5** for other explanations.

Factor	ACE	$-\Delta A_n/\Delta C_{i\text{-}lrc}$	AQY	*dsf*
Species	$P < 0.001$	$P < 0.001$	$P < 0.001$	$P < 0.001$

Table S5. ANOVA *P*-values for the effects of species and C_a (leaf surface CO_2 concentration) on $\Delta A_n/\Delta C_i$ (the slope of a line at the same C_a and different PARs). Species include balsam poplar, black cottonwood and white birch. Here $\Delta A_n/\Delta C_i$ involved *dsf*100, *dsf*150, *dsf*200 from Laisk data and $\Delta A_n/\Delta C_{i\text{-}lrc}$ from light response curve measurement under 400 μmol·mol^{-1} C_a.

Factor	$\Delta A_n/\Delta C_i$
Species	**<0.001**
C_a	0.143
Species X C_a	0.548

Table S6. ANOVA *P*-value for the effects of estimation method and species on R_d, C_i^* and g_m based on Laisk dataset. The three estimation methods are the conventional average midpoint method (Laisk, 1977), the slope-intercept method (Walker *et al.*, 2016) and our vertical line method. The species used include balsam poplar, black cottonwood and white birch.

Factor	R_d	C_i^*	g_m
Method	0.906	0.732	**$P < 0.001$**
Species	**$P < 0.001$**	**$P < 0.001$**	**$P < 0.001$**
Method X Species	0.885	0.882	0.565

Table S7. R_d and C_i^* estimates using the conventional average midpoint method (MP), the slope-intercept method (SI) and our vertical line method (VL) from the same A/C_i measurements at 50, 130 and 240 μmol·m^{-2}·s^{-1} PAR (*i.e.*, Walker's dataset) except for SI-5 which used two additional sets of A/C_i measurements at 420 and 800 μmol·m^{-2}·s^{-1} PAR.

Parameter	Estimation Method			
	MP	VL	SI	SI-5
R_d	0.54	0.52	0.51	0.63
C_i^*	34.8	35.1	35.3	35.4